One dimensional energy transfer in lanthanoid picolinates. Correlation of structure and spectroscopy

Dorota Sendor,[a] Matthias Hilder,[b] Thomas Juestel,[c] Peter C. Junk*[b] and Ulrich H. Kynast*[a]

[a] *Fachhochschule Muenster, Fachbereich Chemieingenieurwesen, Stegerwaldstr. 39, 48 565 Steinfurt, Germany*
[b] *School of Chemistry, Monash University, P.O. Box 23, Clayton Victoria 3800, Australia. E-mail: peter.junk@sci.monash.edu.au; Fax: 61-3-9905 4597*
[c] *Philips Research Laboratories Aachen, Weisshausstr. 2, D-52066 Aachen, Germany*

Received (in London, UK) 25th February 2003, Accepted 16th May 2003
First published as an Advance Article on the web 12th June 2003

Optical and structural properties of rare earth complexes with 2-pyridine carboxylic acid ('Hpic') are evaluated by luminescence spectroscopy, decay measurements, X-ray crystal structure determination, FTIR, DTA and metal content analysis. Corresponding $Tb^{3+}$and Eu^{3+} complexes of this ligand are extraordinarily efficient with respect to their luminescence. In the crystalline state the series is isostructural and composed of $M[Ln(pic)_4]\cdot nH_2O$ (M = Na, NH_4; Ln = Eu, Gd, Tb, Ho) with pic-linked $[Ln(pic)_4]^-$ units forming a chain-like structure, which gives rise to a one-dimensional exchange communication between the rare earth ions; this energy transfer being confined to the chains. Energy transfer of the Coulomb type between the ligands appears to be of significance only, if suitable rare earth acceptor states are not accessible, as is shown for a series of $[La(pic)_4]^-$ series, in which La^{3+} is gradually substituted by Tb^{3+} or Eu^{3+}.

Introduction

Interest in optically active metallo-organic complexes, especially of the rare earths, has been stimulated recently due to potential applications in novel electro-optical devices[1] such as organic light emitting diodes (OLEDs),[2] components in solar cells,[3] sensors,[4] and luminescent immunoassays.[5] Complexes of the rare earths are of particular interest in light generation or transformation devices, where their inherently advantageous emissive properties (line emission, large apparent Stokes shift, high quantum yields, long decay times) are exploited; examples include OLEDs or the combination of solid state blue and UV-light emitting diodes, where they may serve to transpose or adjust the primary LED emission colour. Additionally, rare earth centered metallo-organic complexes have been used to render various types of matrices like sol–gel materials,[6] zeolites[7] or polymers[8] luminescentally active, thus giving access to new classes of luminescent materials.

Although the principal 'local' intramolecular luminescence mechanism of the complexes is well understood, especially in β-diketonates,[9] where the ligand to rare earth energy transfer[10] as well as structural design features may be put on a semi-quantitative basis,[11] a thorough description of the underlying interdependence between optical performance and structure, and on intermolecular and various degrees of interactions with host matrices, appears to be lacking.

Although the possibility and use of intermolecular energy transfer in pure metallo-organic complexes *e.g.* between Eu^{3+} and Tb^{3+} has previously been recognized both for solutions[12] and the solid state,[13] it has not been observed for aromatic carboxylates of the rare earths. Generally, they form polymeric associates[14] with corresponding short range interactions rather than isolated molecular entities, unless co-coordinated by chelating ligands, (although a monomeric exception has been reported, $[Dy(pic)_3(H_2O)_2]\cdot 2.8H_2O$).[15] Similar to the closely related β-diketonates, many aromatic carboxylates are some of the most efficiently luminescing rare earth species. Thus, we report herein, the synthesis and structural characterisation of the isomorphous $Na[Ln(pic)_4]\cdot 1.5H_2O$ series (Ln = Eu (**1**), Gd (**2**), Tb (**3**) and Ho (**5**)) and luminescence spectroscopy of the Ln = Eu, Tb complexes. We also present the synthesis and X-ray crystal structure of the closely related $NH_4[Tb(pic)_4]\cdot 2H_2O$ (**4**).

Results and discussion

Compounds **1**–**3** and **5** were conveniently synthesised in good yield by treatment of an aqueous solution of the respective lanthanoid chloride with sodium picolinate (eqn. (1)). Compound **4** was prepared by treating an aqueous solution of terbium chloride with four equivalents of ammonium picolinate (eqn. (2)).

$$LnCl_3\cdot n(H_2O) + 4Na(pic) \xrightarrow{H_2O} Na[Ln(pic)_4]\cdot 1.5H_2O + 3NaCl \quad (1)$$

$$TbCl_3\cdot n(H_2O) + 4NH_4(pic) \xrightarrow{H_2O} NH_4[Tb(pic)_4]\cdot 2H_2O + 3NH_4Cl \quad (2)$$

There also exists a third modification of composition $Ln(pic)_3$, which is obtained as an anhydrous product derived from the same synthesis depicted in eqn. (1). This species was the only product obtained in the case of Ln = La; but when doping La^{3+} into $[Ln(pic)_4]^-$ (Ln = Eu, Tb) the anionic structure is maintained, as evident from the vibrational spectra. Since the structural change is also accompanied by a noticeable decrease in solubility, the lanthanum containing complexes most likely assume a polymeric structure, whose linkages, in contrast to $Na[Tb_{1-n},Eu_n(pic)_4]$ cannot readily be broken. Single crystals obtained for this series are obtained as micro-crystalline acicular materials, and an X-ray crystal structure determination has thus far been elusive.

 DOI: 10.1039/b302499g

All complexes were characterized by FTIR spectroscopy with pertinent features being a shift of the carbonyl stretching frequencies compared with free ligand. In picolinic acid, the C=O stretches occur at 1718 and 1640 cm^{-1}, whereas in complexes **1**–**5**, these bands are significantly shifted to lower wave numbers (1620 and 1385 cm^{-1} respectively). A splitting into three components, as expected from the crystal structure is not clearly seen, but indicated by a high energy shoulder of the 1385 cm^{-1} absorption. In the presence of the ammonium cation, additional bands occur at 3132 and 1402 cm^{-1} to be assigned to NH stretches and deformation modes. In complexes (**1**–**5**) distinct absorbances appear at 1595 and 1568 cm^{-1} (predominantly $\nu_{C=C}$ in character) and 1474 and 1443 cm^{-1} (predominantly $\nu_{C=N}$ in character), and a broad absorbance is observed at *ca.* 3390 cm^{-1} (O–H stretch). The broad O–H stretching features above 2600 cm^{-1} in the free ligand are absent in spectra of all complexes. In the third type of complex mentioned above ($Ln(pic)_3$), the C=O stretches are shifted to 1651 and 1338 cm^{-1}, while the vibrations of the ring system remain practically the same. Complexes (**1**)–(**5**) were pure by Na_2EDTA titration for lanthanoid content, and water content (DTA). Compounds **1** to **5** show good thermal stability up to 250 °C where they begin to show signs of decomposition. In DTA/DTG measurements, carried out on $Na[Tb(pic)_4]\cdot 1.5H_2O$ the onset of decomposition occurs at 246 °C (weight loss 20.65% corresponding to $1.5H_2O$ and one $C_5H_5NCO_2H$, exothermal), a final decomposition accompanied with a weight loss of 70% (endothermal) is found at 398 °C. The lanthanum complex of unknown structure does not show any weight loss up to 398 °C, after which decomposition takes place (55.3% mass loss is observed).

X-ray crystal structures were performed on complexes **1**–**5** and in each case, the complexes were isostructural, crystallizing in the hexagonal space group $P6_522$. The overall structures exhibit single-strand polymeric chains of $[Ln(pic)_4]^-$ units interconnected *via* a bridging picolinate ligand, with Na^+ (for compounds **1**–**3** and **5**) or NH_4^+ (for compound **4**) cations binding in clefts along the polymeric chain and water molecules completing the coordination sphere about the Na^+ or NH_4^+ cations (Figs. 1 and 2). The Na^+ and NH_4^+ cations also bridge between adjacent $[Ln(pic)_4]^-$ anions by bridging between successive $O_{(carboxylate)}$ atoms. Previously, lanthanoid structures with the picolinate ligand have been determined for Dy^{3+} (see above), polymeric $[H_3N{-}CH_2CH_2{-}NH_3]^{2+}$ $[Ho_2(pic)_8]^{2-}$[16] and the analogous Nd^{3+} complex.[17] With regard to the metal ion coordination, we find the metal centre in all structures most closely resembles doubled trigonal prism geometry.[18] The nine-coordination is made up of four chelating (through the pyridyl nitrogen and carboxylate oxygen atoms) picolinate ligands and one oxygen atom of a bridging carboxylate ligand. The sodium centre is five coordinate, being bound by four carboxylate oxygen atoms (which bridge to Ln centres) and one water oxygen atom. All Ln–O, Ln–N and Na–O distances are unexceptional (Tables 1 to 5). The

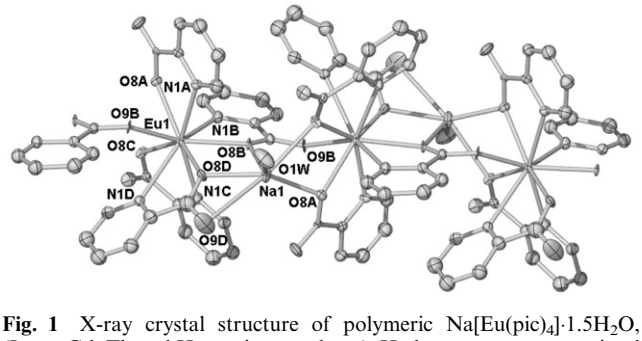

Fig. 1 X-ray crystal structure of polymeric $Na[Eu(pic)_4]\cdot 1.5H_2O$, (Ln = Gd, Tb and Ho are isomorphous). Hydrogen atoms are omitted for clarity. Thermal ellipsoids are at the 30% probability level.

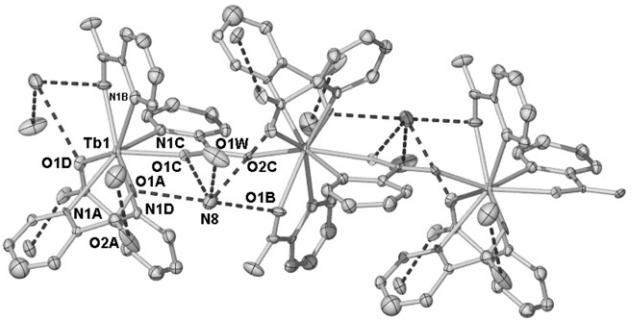

Fig. 2 X-ray crystal structure of polymeric $NH_4[Tb(pic)_4]\cdot 2H_2O$. Hydrogen atoms are omitted for clarity. Thermal ellipsoids are at the 30% probability level.

Ln–O and Ln–N distances show a gradual general diminishment in length (*ca.* 0.03 Å and 0.05 Å respectively) in moving from Eu to Ho as is expected for the lanthanoid contraction.[19] Ln···Ln-distances, which are essential criteria in luminescence chemistry of the lanthanoids where metal–metal quenching can be of paramount importance, are all in the vicinity of *ca.* 6.34 Å and should discount any bonding communication between the metal centres. A further salient feature of these structures is the absence of any Ln–H_2O interactions which can have repercussions in the photophysics of the complexes.

The Tb^{3+} and Eu^{3+} complexes exhibit very efficient luminescence both in the solid state and in solution and are thus of immediate interest in the context outlined above. For solid

Table 1 Selected (i) bond distances (Å), (ii) angles (°), for $Na[Eu(pic)_4]\cdot 1.5H_2O$, **1**

(i) Atoms	Distance	Atoms	Distance
Eu(1)–O(8A)	2.413(11)	Na(1)–O(1W)	2.32(2)
Eu(1)–O(8B)	2.461(9)	Na(1)–O(8A)#2	2.341(14)
Eu(1)–O(8C)	2.358(10)	Na(1)–O(8B)	2.543(13)
Eu(1)–O(8D)	2.326(13)	Na(1)–O(8C)#2	2.598(14)
Eu(1)–O(9B)	2.390(10)	Na(1)–O(8D)	2.377(14)
Eu(1)–N(1A)	2.625(13)	Na(1)–O(9D)	2.98(2)
Eu(1)–N(1B)	2.624(15)	Eu(1)–Na(1)	4.046(8)
Eu(1)–N(1C)	2.604(15)	Eu(1)–Na(1)#1	3.798(8)
Eu(1)–N(1D)	2.691(15)		

(ii) Atoms	Angle	Atoms	Angle
O(8A)–Eu(1)–O(8B)	114.4(4)	O(8C)–Eu(1)–N(1A)	137.7(4)
O(8A)–Eu(1)–O(8C)	74.0(4)	O(8C)–Eu(1)–N(1B)	74.9(4)
O(8A)–Eu(1)–O(8D)	143.9(5)	O(8C)–Eu(1)–N(1C)	64.2(4)
O(8A)–Eu(1)–O(9B)	72.2(4)	O(8C)–Eu(1)–N(1D)	73.9(4)
O(8A)–Eu(1)–N(1A)	64.2(4)	O(8D)–Eu(1)–O(9B)	84.8(5)
O(8A)–Eu(1)–N(1B)	70.9(5)	O(8D)–Eu(1)–N(1A)	82.2(5)
O(8A)–Eu(1)–N(1C)	129.8(4)	O(8D)–Eu(1)–N(1B)	128.8(5)
O(8A)–Eu(1)–N(1D)	125.5(4)	O(8D)–Eu(1)–N(1C)	86.2(5)
O(8B)–Eu(1)–O(8C)	128.5(4)	O(8D)–Eu(1)–N(1D)	64.3(4)
O(8B)–Eu(1)–O(8D)	67.2(4)	O(9B)–Eu(1)–N(1A)	70.2(4)
O(8B)–Eu(1)–O(9B)	139.7(4)	O(9B)–Eu(1)–N(1B)	142.9(5)
O(8B)–Eu(1)–N(1A)	77.6(4)	O(9B)–Eu(1)–N(1C)	132.7(5)
O(8B)–Eu(1)–N(1B)	62.7(4)	O(9B)–Eu(1)–N(1D)	66.0(4)
O(8B)–Eu(1)–N(1C)	75.7(4)	N(1A)–Eu(1)–N(1B)	96.5(5)
O(8B)–Eu(1)–N(1D)	120.1(4)	N(1A)–Eu(1)–N(1C)	153.2(4)
O(8C)–Eu(1)–O(8D)	135.6(4)	N(1A)–Eu(1)–N(1D)	126.0(4)
O(8C)–Eu(1)–O(9B)	91.8(4)	N(1B)–Eu(1)–N(1C)	72.4(5)
		N(1B)–Eu(1)–N(1D)	137.5(5)
		N(1C)–Eu(1)–N(1D)	68.3(5)

Symmetry transformations used to generate equivalent atoms: **#1** $x-y, -y+1, -z$ **#2** $x-y+1, -y+1, -z$

Table 2 Selected (i) bond distances (Å), (ii) angles (°), for Na[Gd(pic)$_4$]·1.5H$_2$O, **2**

(i)

Atoms	Distance	Atoms	Distance
Gd(1)–O(8A)	2.405(11)	Na(1)–O(1W)	2.26(2)
Gd(1)–O(8B)	2.453(10)	Na(1)–O(8A)#2	2.363(15)
Gd(1)–O(8C)	2.347(11)	Na(1)–O(8B)	2.548(13)
Gd(1)–O(8D)	2.333(12)	Na(1)–O(8C)#2	2.602(15)
Gd(1)–O(9B)	2.365(10)	Na(1)–O(8D)	2.373(14)
Gd(1)–N(1A)	2.627(14)	Na(1)–O(9D)	3.02(2)
Gd(1)–N(1B)	2.615(16)	Gd(1)–Na(1)	4.038(8)
Gd(1)–N(1C)	2.582(16)	Gd(1)–Na(1)#1	3.803(8)
Gd(1)–N(1D)	2.689(15)		

(ii)

Atoms	Angle	Atoms	Angle
O(8A)–Gd(1)–O(8B)	113.5(4)	O(8C)–Gd(1)–N(1A)	137.5(4)
O(8A)–Gd(1)–O(8C)	74.3(4)	O(8C)–Gd(1)–N(1B)	75.1(4)
O(8A)–Gd(1)–O(8D)	143.9(5)	O(8C)–Gd(1)–N(1C)	64.8(4)
O(8A)–Gd(1)–O(9B)	72.4(4)	O(8C)–Gd(1)–N(1D)	73.7(4)
O(8A)–Gd(1)–N(1A)	63.8(4)	O(8D)–Gd(1)–O(9B)	84.7(4)
O(8A)–Gd(1)–N(1B)	70.3(5)	O(8D)–Gd(1)–N(1A)	82.4(5)
O(8A)–Gd(1)–N(1C)	130.7(4)	O(8D)–Gd(1)–N(1B)	129.1(4)
O(8A)–Gd(1)–N(1D)	125.7(5)	O(8D)–Gd(1)–N(1C)	85.3(5)
O(8B)–Gd(1)–O(8C)	128.9(4)	O(8D)–Gd(1)–N(1D)	64.2(4)
O(8B)–Gd(1)–O(8D)	67.5(4)	O(9B)–Gd(1)–N(1A)	69.6(4)
O(8B)–Gd(1)–O(9B)	139.1(4)	O(9B)–Gd(1)–N(1B)	142.5(5)
O(8B)–Gd(1)–N(1A)	77.3(4)	O(9B)–Gd(1)–N(1C)	132.7(5)
O(8B)–Gd(1)–N(1B)	62.8(4)	O(9B)–Gd(1)–N(1D)	66.2(4)
O(8B)–Gd(1)–N(1C)	76.1(4)	N(1A)–Gd(1)–N(1B)	96.4(5)
O(8B)–Gd(1)–N(1D)	120.7(4)	N(1A)–Gd(1)–N(1C)	153.3(5)
O(8C)–Gd(1)–O(8D)	135.3(4)	N(1A)–Gd(1)–N(1D)	125.9(4)
O(8C)–Gd(1)–O(9B)	91.9(4)	N(1B)–Gd(1)–N(1C)	73.4(5)
		N(1B)–Gd(1)–N(1D)	137.7(5)
		N(1C)–Gd(1)–N(1D)	67.8(5)

Symmetry transformations used to generate equivalent atoms: **#1** $x-y, -y+1, -z$ **#2** $x-y+1, -y+1, -z$

Table 3 Selected (i) bond distances (Å), (ii) angles (°), for Na[Tb(pic)$_4$]·1.5H$_2$O, **3**

(i)

Atoms	Distance	Atoms	Distance
Tb(1)–O(8A)	2.396(9)	Na(1)–O(1W)	2.293(15)
Tb(1)–O(8B)	2.435(8)	Na(1)–O(8A)#2	2.350(11)
Tb(1)–O(8C)	2.339(8)	Na(1)–O(8B)	2.521(10)
Tb(1)–O(8D)	2.324(9)	Na(1)–O(8C)#2	2.580(11)
Tb(1)–O(9B)	2.384(9)	Na(1)–O(8D)	2.373(11)
Tb(1)–N(1A)	2.586(11)	Na(1)–O(9D)	2.946(17)
Tb(1)–N(1B)	2.622(12)	Tb(1)–Na(1)	4.035(6)
Tb(1)–N(1C)	2.571(12)	Tb(1)–Na(1)#1	3.794(6)
Tb(1)–N(1D)	2.683(12)		

(ii)

Atoms	Angle	Atoms	Angle
O(8A)–Tb(1)–O(8B)	114.3(3)	O(8C)–Tb(1)–N(1A)	137.7(3)
O(8A)–Tb(1)–O(8C)	73.6(3)	O(8C)–Tb(1)–N(1B)	75.2(3)
O(8A)–Tb(1)–O(8D)	143.4(4)	O(8C)–Tb(1)–N(1C)	65.8(3)
O(8A)–Tb(1)–O(9B)	72.3(3)	O(8C)–Tb(1)–N(1D)	74.8(3)
O(8A)–Tb(1)–N(1A)	64.6(3)	O(8D)–Tb(1)–O(9B)	84.7(4)
O(8A)–Tb(1)–N(1B)	70.6(4)	O(8D)–Tb(1)–N(1A)	81.3(4)
O(8A)–Tb(1)–N(1C)	130.7(3)	O(8D)–Tb(1)–N(1B)	128.9(3)
O(8A)–Tb(1)–N(1D)	125.5(4)	O(8D)–Tb(1)–N(1C)	85.8(4)
O(8B)–Tb(1)–O(8C)	129.3(3)	O(8D)–Tb(1)–N(1D)	64.1(3)
O(8B)–Tb(1)–O(8D)	66.9(3)	O(9B)–Tb(1)–N(1A)	70.9(3)
O(8B)–Tb(1)–O(9B)	139.5(3)	O(9B)–Tb(1)–N(1B)	142.8(4)
O(8B)–Tb(1)–N(1A)	76.6(3)	O(9B)–Tb(1)–N(1C)	132.9(4)
O(8B)–Tb(1)–N(1B)	62.9(3)	O(9B)–Tb(1)–N(1D)	65.2(3)
O(8B)–Tb(1)–N(1C)	75.2(3)	N(1A)–Tb(1)–N(1B)	95.9(4)
O(8B)–Tb(1)–N(1D)	120.2(3)	N(1A)–Tb(1)–N(1C)	151.7(4)
O(8C)–Tb(1)–O(8D)	136.4(4)	N(1A)–Tb(1)–N(1D)	125.3(3)
O(8C)–Tb(1)–O(9B)	91.2(3)	N(1B)–Tb(1)–N(1C)	72.9(4)
		N(1B)–Tb(1)–N(1D)	138.7(4)
		N(1C)–Tb(1)–N(1D)	69.2(4)

Symmetry transformations used to generate equivalent atoms: **#1** $x-y, -y+1, -z$ **#2** $x-y+1, -y+1, -z$

samples we determined the quantum yield to be 74% under 254 nm excitation; the extrapolation of excitation intensities and reflectance as well as the decay times indicate quantum yields of Na[Tb(pic)$_4$] near unity at 285 nm excitation; the corresponding Na[Eu(pic)$_4$] is determined spectroscopically to be of somewhat lower efficiency (approx. 50% at 285 nm), although lifetime measurements suggest even higher quantum yields (see below). Typical optical spectra of the Eu^{3+} and Tb^{3+} picolinates are depicted in Fig. 3.

Excitation occurs *via* an allowed ligand singlet $^1S_0 \rightarrow {}^1S^*$ absorption, followed by intersystem crossing (ISC) to the ligand triplet ^3T, the ISC being promoted by spin orbit coupling due to the nearby lanthanoid. It is known that the triplet state may very efficiently transfer its energy to the lanthanoid, if it possesses states suitable for overlap, *i.e.* matching energy.[9] This match is obviously given in the case of the $Tb^{3+}(^5D_4)$ level in $[Tb(pic)_4]^-$, which contributes to the high efficiency of the complex, whereas in $[Eu(pic)_4]^-$, the $Eu^{3+}(^5D_1)$ and $(^5D_0)$ levels are at lower energy, thus causing a lower intramolecular transfer rate.

Furthermore, by consecutively substituting Eu^{3+} for Tb^{3+} in $NH_4[Tb(pic)_4]$, we were able to extract data on the parameters for Ln–Ln energy transfer in correlation to the structural information. The stepwise substitution of Tb^{3+} by Eu^{3+} in this system is a particularly suitable monitor, firstly, because the complexes of both Tb^{3+} and Eu^{3+} show efficient luminescence. Furthermore, free $(NH_4)[Eu(pic)_4]$ and the derived $(NH_4)[Tb_nEu_{1-n}(pic)_4]$ mixtures possess identical structures, as evident from their IR-spectra. Additionally, the crystal structures of the isostructural $(NH_4)[Ln(pic)_4]$ and $Na[Ln(pic)_4]$ reveal absence of water coordination to the rare earth ions (see above), which is of particular significance for the Eu^{3+} ion, since deactivations due to high frequency vibrations can thus be excluded.

In the first instance, the mixed $(NH_4)[Tb,Eu(pic)_4]$ materials were excited at 490 nm, corresponding to $Tb^{3+}(^7F_6–{}^5D_4)$ excitation. The excited $Tb^{3+}(^5D_4)$ state can then transfer its energy into the Eu $(^5D_1)$ level. After an internal relaxation step, $Eu^{3+}(^5D_0–{}^7F_2)$ emission can be monitored at 612 nm, as the $Eu^{3+}(^5D_0)$ state is efficiently emissive in the picolinates. At the same time, the intensity of the $Tb^{3+}(^5D_4 \rightarrow {}^7F_5)$ emission at 545 nm will be reduced, if the transfer takes place. The intensity ratios between the Tb^{3+} and Eu^{3+} emission at different Tb^{3+}/Eu^{3+} contents thus reflect the energy transfer efficiency. For a 50% substitution of Tb^{3+} *vs.* Eu^{3+} a decline of the Tb^{3+} emission intensity to 50% will be monitored in the absence of energy transfer, whereas in the presence of transfer, the Tb^{3+} emission intensity is expected to be lowered below 50%, depending on the transfer efficiency. As depicted in Fig. 4, the depreciation of the Tb^{3+} emission to 50% is already obtained at a surprisingly low substitution level of less than 10%, clearly indicating the strong exchange interaction $Tb^{3+}(^5D_4) \leftrightarrow$ Eu $(^5D_1)$. The emission spectra obtained for the 50% and 10% substitution of Tb^{3+} with Eu^{3+} in $NH_4[Tb(pic)_4]\cdot1.5H_2O$ are shown in Fig. 5. It is of interest that excitation at 280 nm, which corresponds to ligand excitation, results in almost exactly the same dependence, which is in agreement with the hypothesis that in the presence of suitable acceptor states to the ligand triplet level, energy transfer predominantly occurs through the

Table 4 Selected (i) bond distances (Å), (ii) angles (°), for $NH_4[Tb(pic)_4]\cdot 2H_2O$, **4**

(i)

Atoms	Distance	Atoms	Distance
Tb(1)–O(1A)	2.328(13)	Tb(1)–N(1A)	2.751(14)
Tb(1)–O(1B)	2.384(15)	Tb(1)–N(1B)	2.640(18)
Tb(1)–O(1C)	2.338(12)	Tb(1)–N(1C)	2.637(17)
Tb(1)–O(2C)#1	2.273(15)	Tb(1)–N(1D)	2.566(17)
Tb(1)–O(1D)	2.347(13)		

(ii)

Atoms	Angle	Atoms	Angle
O(1A)–Tb(1)–O(1B)	140.1(6)	O(1C)–Tb(1)–N(1A)	124.1(5)
O(1A)–Tb(1)–O(1C)	69.0(4)	O(1C)–Tb(1)–N(1B)	74.0(5)
O(1A)–Tb(1)–O(1D)	132.7(5)	O(1C)–Tb(1)–N(1C)	63.4(5)
O(1A)–Tb(1)–O(2C)#1	87.1(5)	O(1C)–Tb(1)–N(1D)	75.8(5)
O(1A)–Tb(1)–N(1A)	63.9(4)	O(1D)–Tb(1)–O(2C)#1	91.7(5)
O(1A)–Tb(1)–N(1B)	79.6(6)	O(1D)–Tb(1)–N(1A)	72.5(5)
O(1A)–Tb(1)–N(1C)	129.7(5)	O(1D)–Tb(1)–N(1B)	143.0(6)
O(1A)–Tb(1)–N(1D)	81.9(5)	O(1D)–Tb(1)–N(1C)	73.0(5)
O(1B)–Tb(1)–O(1C)	105.4(5)	O(1D)–Tb(1)–N(1D)	65.9(5)
O(1B)–Tb(1)–O(1D)	82.8(6)	O(2C)#1–Tb(1)–N(1A)	66.1(5)
O(1B)–Tb(1)–O(2C)#1	72.1(6)	O(2C)#1–Tb(1)–N(1B)	69.5(5)
O(1B)–Tb(1)–N(1A)	130.0(5)	O(2C)#1–Tb(1)–N(1C)	141.0(5)
O(1B)–Tb(1)–N(1B)	61.4(6)	O(2C)#1–Tb(1)–N(1D)	134.6(5)
O(1B)–Tb(1)–N(1C)	70.6(6)	N(1A)–Tb(1)–N(1B)	122.6(5)
O(1B)–Tb(1)–N(1D)	136.6(6)	N(1A)–Tb(1)–N(1C)	136.0(5)
O(1C)–Tb(1)–O(1D)	128.8(5)	N(1A)–Tb(1)–N(1D)	69.5(5)
O(1C)–Tb(1)–O(2C)#1	139.3(5)	N(1B)–Tb(1)–N(1C)	101.4(6)
		N(1B)–Tb(1)–N(1D)	148.7(5)
		N(1C)–Tb(1)–N(1D)	72.0(5)

Symmetry transformations used to generate equivalent atoms: **#1** $x-y+1, -y+1, -z$

Table 5 Selected (i) bond distances (Å), (ii) angles (°), for $Na[Ho(pic)_4]\cdot 1.5H_2O$, **5**

(i)

Atoms	Distance	Atoms	Distance
Ho(1)–O(8A)	2.322(7)	Na(1)–O(1W)	2.307(13)
Ho(1)–O(8B)	2.351(7)	Na(1)–O(8A)	2.576(9)
Ho(1)–O(8C)	2.367(7)	Na(1)–O(8C)	2.327(10)
Ho(1)–O(8D)	2.292(7)	Na(1)–O(8D)#2	2.405(9)
Ho(1)–O(9B)	2.405(7)	Na(1)–O(9B)#2	2.515(9)
Ho(1)–N(1A)	2.552(10)	Na(1)–O(9D)#3	3.026(9)
Ho(1)–N(1B)	2.600(10)	Ho(1)–Na(1)	3.775(5)
Ho(1)–N(1C)	2.583(9)	Ho(1)–Na(1)#1	4.030(5)
Ho(1)–N(1D)	2.673(10)		

(ii)

Atoms	Angle	Atoms	Angle
O(8A)–Ho(1)–O(8B)	90.8(3)	O(8C)–Ho(1)–N(1A)	131.2(3)
O(8A)–Ho(1)–O(8C)	73.5(3)	O(8C)–Ho(1)–N(1B)	71.0(3)
O(8A)–Ho(1)–O(8D)	135.8(3)	O(8C)–Ho(1)–N(1C)	65.3(3)
O(8A)–Ho(1)–O(9B)	130.2(2)	O(8C)–Ho(1)–N(1D)	124.9(3)
O(8A)–Ho(1)–N(1A)	66.1(3)	O(8D)–Ho(1)–O(9B)	67.2(3)
O(8A)–Ho(1)–N(1B)	75.0(3)	O(8D)–Ho(1)–N(1A)	85.1(3)
O(8A)–Ho(1)–N(1C)	138.1(3)	O(8D)–Ho(1)–N(1B)	129.3(3)
O(8A)–Ho(1)–N(1D)	73.7(3)	O(8D)–Ho(1)–N(1C)	80.8(3)
O(8B)–Ho(1)–O(8C)	72.2(3)	O(8D)–Ho(1)–N(1D)	64.5(3)
O(8B)–Ho(1)–O(8D)	84.5(3)	O(9B)–Ho(1)–N(1A)	76.3(3)
O(8B)–Ho(1)–O(9B)	138.9(3)	O(9B)–Ho(1)–N(1B)	63.4(3)
O(8B)–Ho(1)–N(1A)	132.2(3)	O(9B)–Ho(1)–N(1C)	76.3(3)
O(8B)–Ho(1)–N(1B)	143.0(3)	O(9B)–Ho(1)–N(1D)	121.1(3)
O(8B)–Ho(1)–N(1C)	70.1(3)	N(1A)–Ho(1)–N(1B)	73.2(4)
O(8B)–Ho(1)–N(1D)	65.3(3)	N(1A)–Ho(1)–N(1C)	152.3(3)
O(8C)–Ho(1)–O(8D)	143.6(3)	N(1A)–Ho(1)–N(1D)	68.1(3)
O(8C)–Ho(1)–O(9B)	114.0(3)	N(1B)–Ho(1)–N(1C)	97.8(3)
		N(1B)–Ho(1)–N(1D)	137.4(3)
		N(1C)–Ho(1)–N(1D)	124.8(3)

Symmetry transformations used to generate equivalent atoms: **#1** $x-y, -y+1, -z$ **#2** $x-y+1, -y+1, -z$ **#3** $1+x-y, 1-y, -z$

$[Tb^{3+}(^5D_4)] \rightarrow [Eu^{3+}(^5D_1)]$ channel rather than [pic(on Tb^{3+})] → [pic(on Eu^{3+})] → $[Eu^{3+}(^5D_1)]$ or [pic(on Tb^{3+})] → $[Eu^{3+}(^5D_1)]$.

The decay times measured for this series with regard to the depreciation of the Tb^{3+} emission signal at 545 nm clearly support this picture. The pure samples as well as $NH_4[Tb_{0.9}Eu_{0.1}(pic)_4]$, as given in Fig. 6, could be fitted as single exponentials. $NH_4[Tb_{0.5}Eu_{0.5}(pic)_4]$ (not represented) had two components in the $Tb^{3+}(^5D_4)$ emission, the lifetimes of which were obtained as $\tau_1 = 0.303$ (±0.034) ms and $\tau_2 = 1.275$ (±0.17) ms. For $[Tb(pic)_4]^-$ and $[Eu(pic)_4]^-$ the decay times determined amount to 1.639 (±0.001) ms and 1.603 (±0.002) ms respectively, which is in reasonable agreement with the quantum yields determined from the spectral measurements; the lifetime of the mixed complex $NH_4[Tb_{0.9}Eu_{0.1}(pic)_4]$ is obtained as 0.789 (±0.002) ms at 545 nm. For a comparison, in the diketenato complex $Eu(tta)_3\cdot dbso$ (tta = thenyltrifluoracetylacetone, dbso = dibenzoylsulfoxide), a lifetime of 1.4 ms corresponding to a quantum yield of 85% has been reported.[20]

If in this same series the decay of the Eu^{3+} instead of of the Tb^{3+} signal is measured at 612 nm, we initially observe an increase of the $Eu^{3+}(^5D_0)$ lifetime to *e.g.* 1.974 (±0.006) ms at 10% substitution with Eu^{3+}, which at 50% and 1.663 (±0.002) ms still is somewhat longer than for pure $[Eu(pic)_4]^-$ (1.603 (±0.002) ms; all Eu^{3+} decays could be fitted mono-exponentially). We interpret this initial increase at low Eu^{3+} concentrations as a consequence of the absence of energy migration between the Eu^{3+} ions, which increases accordingly at higher Eu^{3+} content, thus giving rise to some concentration quenching eventually. It should be noted that this interpretation also conforms with the slight depreciation of the Eu^{3+} emission intensities observed above *ca.* 50% Eu^{3+} content in the series depicted in Figs. 4,5.

Similarly, energy migration $Tb^{3+} \rightarrow Tb^{3+}$ also appears likely. In view of the chain structure in the solid, at a Eu^{3+} substitution level of 10%, the average distance between two nearest Eu^{3+} ions in a chain amounts to 63.4 Å, in between which nine Tb^{3+} ions are accommodated. As each of these Tb^{3+} ions has the same probability of capturing the incident photon, and 50% of the excitation energy reach a Eu^{3+} ion, on average it will have traversed a distance of *ca.* 12.65 Å. This is pronouncedly more than can be expected for exchange interaction transfer, thus, about two Tb^{3+} ions have been involved intermediately.

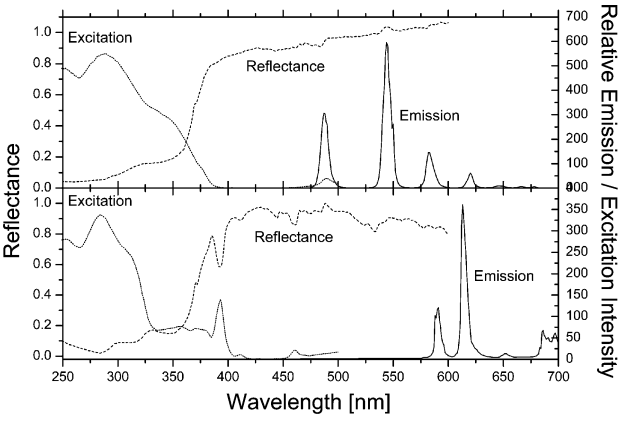

Fig. 3 Optical spectra of $Na[Tb(pic)_4]\cdot 1.5H_2O$ (upper spectrum) and $Na[Eu(pic)_4]\cdot 1.5H_2O$ (lower spectrum).

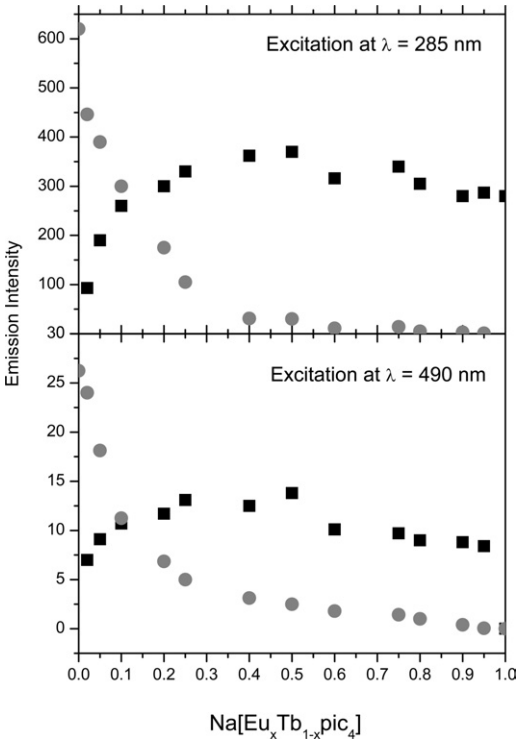

Fig. 4 Emission intensities on stepwise substitution of Tb^{3+} with Eu^{3+} in $NH_4[Tb(pic)_4]\cdot 1.5H_2O$; circles Emission at 545 nm (Tb^{3+}), squares at 612 nm (Eu^{3+}).

We have also sought for intermolecular transfers originating from ligand excitation in this system by substituting La^{3+} for Tb^{3+} in $Na[Tb(pic)_4]$ or Eu^{3+} in $NH_4[Eu(pic)_4]$. Here, a non-linear increase of the Tb^{3+} emission intensity would indicate an 'intermolecular' transfer, the term intermolecular denominating transfer from building units of the polymer chain not being part of a neighbouring one. Intermolecular energy transfer between ligands themselves might be expected, because it would be of the dipole–dipole type (Coulomb interaction) and should thus extend over several molecular units allowing the excitation to probe large volumes for the presence of Tb^{3+} ions. It was therefore somewhat surprising that ligand → ligand energy transfer seems to be of secondary significance at most in the $[Tb,Eu(pic)_4]^-$ system. The data obtained for the $Na[Tb_{1-n},La_n(pic)_4]$ and $Na[Eu_{1-n},La_n(pic)_4]$ series (Fig. 7), however, now clearly comply with a transfer *via* ligands, as indicated by the steep linear increase of the Tb^{3+}

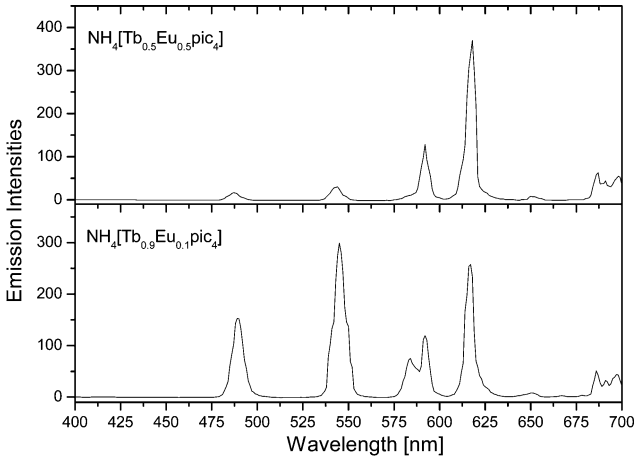

Fig. 5 Emission spectra obtained for 10% and 50% substitution of Tb^{3+} with Eu^{3+} in $NH_4[Tb(pic)_4]\cdot 1.5H_2O$.

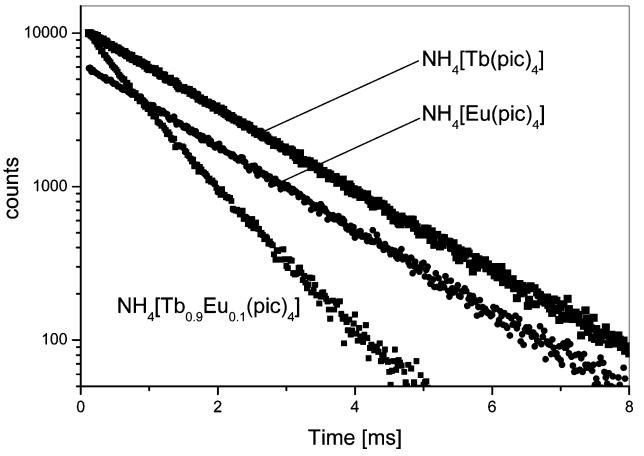

Fig. 6 Decay curves of $NH_4[Tb(pic)_4]\cdot 1.5H_2O$, $NH_4[Eu(pic)_4]\cdot 1.5H_2O$ and $NH_4[Tb_{0.9}Eu_{0.1}(pic)_4]\cdot 1.5H_2O$ excited at 272 nm and monitored at 545 nm (Tb^{3+} containing complexes) and 612 nm for $NH_4[Eu(pic)_4]\cdot 1.5H_2O$.

emission, yielding 50% of the eventual intensity at a low terbium content of only about 10% and *ca.* 5% for the corresponding Eu^{3+} series. It has been highlighted, however, that in this latter series $Na[Tb_{1-n},La_n(pic)_4]$, a structural change is involved, evidenced by *e.g.* the above mentioned shift of the C=O frequencies, such that a further discussion of ligand → ligand transfer will be refrained from here.

With regard to $Tb^{3+} \rightarrow Eu^{3+}$ transfer by exchange interaction, the transfer probability $P_{Tb\rightarrow Eu} = (1/\tau) - (1/\tau_0)$[21] can be estimated to be 0.61 in the sample containing 10 Eu^{3+}, τ being the donor lifetime (Tb^{3+}) in the presence of an acceptor (Eu^{3+}), τ_0 in its absence. The energy transfer efficiency $E_{Tb\rightarrow Eu} = (1 - \tau/\tau_0)$[22] for this sample thus calculates to 0.48 correspondingly.

Following the procedure described in,[23] the number of energy transfer partners n, *viz.* the acceptors (Eu^{3+}),

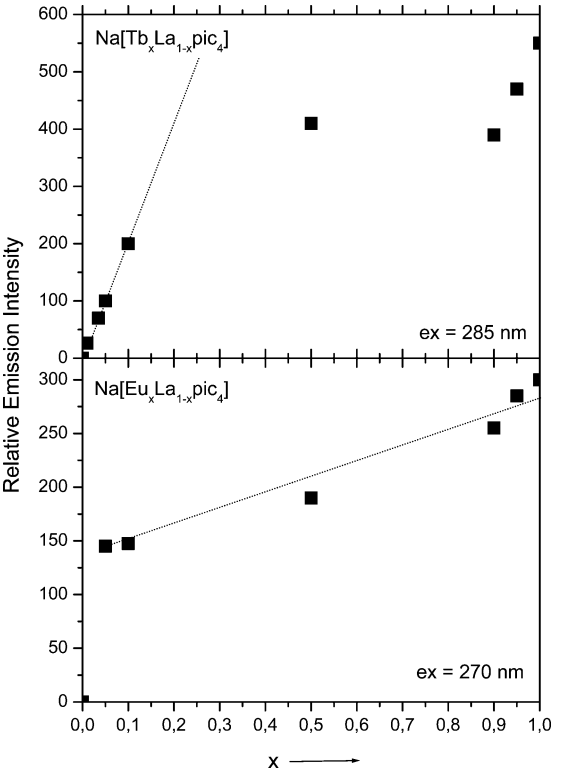

Fig. 7 Emission intensities on stepwise substitution of Tb^{3+}(top) and Eu^{3+} (bottom) with La^{3+} in the complexes $NH_4[Ln(pic)_4]\cdot 1.5H_2O$. See text remarks on structure.

surrounding the Tb^{3+} sites is calculated to be 2 from the $Na[Tb_{1-n},Eu_n(pic)_4]$ series. This figure is obtained independent of the crystal structure and can serve as a proof that transfer occurs within one chain exclusively and not between the strands. Furthermore, using the crystallographic distance of 6.34 Å between neighbouring rare earth ions, the critical transfer radius for this one-dimensional process is obtained as 6.05 Å.[23]

Conclusions

Anionic picolinates of Gd, Tb, Eu and Ho as well as mixed Eu^{3+}/Tb^{3+} complexes have been prepared and characterized structurally and by optical spectroscopy and decay measurements. The solid state structure consists of strands of $[Ln(pic)_4]^-$ ions, which are linked by picolinates bridging *via* carboxylic oxygens, while NH_4^+ or Na^+ cations and water molecules, not directly linked to the lanthanoids, complement the structure. Picolinates of lanthanum and its mixed complexes with Eu^{3+} and Tb^{3+} assume a different structure, most likely with a higher degree of association. In these, spectroscopic evidence for energy transfer channels between ligands is detected.

The complexes of Tb^{3+} and Eu^{3+}, as well as their mixed complexes show very efficient luminescence under UV excitation, the quantum yields approaching 100%. The structural data enabled us to trace the origin and one-dimensional nature of the energy transfer processes observed between Tb^{3+} and Eu^{3+} and to assess the energy transfer parameters. The $Tb^{3+}(^5D_4)$ emission is quenched to 50% by Eu^{3+} at a low substitution level of 10% in mixed complexes. In these, ligand to ligand energy transfer is not observed. The critical transfer radius for $Tb^{3+} \rightarrow Eu^{3+}$ was found to be 6.05 Å. We expect that these findings will have an immediate impact on our ongoing research on metallo-organic complexes embedded in polymeric and nano-structured matrices such as sol–gel and zeolite hosts.

Experimental

Lanthanoid salts and picolinic acid were purchased from Aldrich and used without further purification. Deionised water was used in all syntheses. FT infrared spectra were recorded on sodium chloride plates as Nujol mulls and KBr pellets on a Nicolet Nexus FTIR spectrophotometer and a Perkin-Elmer Spectrum One spectrometer. Lanthanoid metal analyses were determined titrimetrically using the Na_2EDTA method described elsewhere.[24] Melting points were performed in unsealed tubes. For selected samples the water content and thermal stability was determined from DTA/DTG measurements (Netzsch STA 409) at a heating rate of 20 °C min^{-1} and a Al_2O_3 reference in synthetic air.

Optical measurements

Optical spectra of the solid were taken through a quartz plate under excitation with a 150 W Xe lamp, ARC excitation and emission monochromators of 300 mm focal length and detection with a photomultiplier. Reflectance spectra were obtained using an integrating sphere with a diameter of 70 mm and 10 mm port openings *versus* commercial white and black references (Labsphere). The system response was corrected *versus* $BaMgAl_{10}O_{17}$:Eu (BAM) generously provided by Philips Research Laboratories/Aachen. Quantum yields were determined as described elsewhere.[25]

Lifetimes

The spectrometer system (Edinburgh Instr.) for the lifetime measurements is equipped with a μs-flash lamp (μF900, Edinburgh Inst.), which is mounted at the second entrance slit of the excitation monochromator in the Xe-lamp branch. Thus radiation in the spectral range between 220 to 800 nm is available for microsecond decay time measurements. The microsecond flash lamp is a pulsed Xenon filled flash lamp with a typical pulse duration of 2 μs at full width half maximum with repetition rates up to 100 Hz for time correlated single photon counting (TCSPC). The photons of the TCSPC experiment are correlated by a time-to-amplitude converter (TAC) to the excitation light pulse. The TAC provides an output pulse whose voltage is proportional to the time between the start and the stop signal. A multichannel analyzer (MCA) converts this voltage to a time channel. By the summation over many pulses the MCA builds up a probability histogram of counts *versus* time channels. During measurement the whole time window is visible on the MCA screen and the time histogram is displayed in real time on the monitor. The conversion gain of the MCA is adjustable, enabling the measurement with 1024, 2048 and 4096 time channels.

Synthesis

Complexes **1** to **3** and **5** were synthesised following a similar procedure. Thus, *ca.* 2.4 mmol of Na(pic) was added to *ca.* 0.6 mmol $LnCl_3$. The samples were allowed to evaporate until large crystals of the complexes were deposited. Complex **4** was synthesised in a similar manner, except the NH_4(pic) was used in place of Na(pic). Details of the properties for each compound follow. Yields reported are for isolated crystalline material. The significant solubility of the compounds in water is responsible for low yields. Yields of these essentially quantitative reactions can be enhanced by precipitation of the compounds by addition of acetone to a saturated aqueous solution.

IR spectra (KBr pellets or ATR)ν/cm^{-1}. 3400 m (br), (**4** only: 3163 m (br)), 1624 s, 1588 s, 1568 m, 1474 m, 1443 w, (**4** only: 1400 m), 1382 s, 1296 m, 1240 w, 1171 m, 1148 w, 1093 w, 1049 m, 1013 m, 856 m, 761 m, 760 s, 705 s, 633 m.

Analyses. *$Na[Eu(pic)_4]\cdot 1.5H_2O$* (**1**). Yield 55%. $C_{24}H_{19}EuN_4NaO_{9.5}$ requires Eu 22.0%; found Eu 22.6%. M.Pt. > 250 °C (dec.).
$Na[Gd(pic)_4]\cdot 1.5H_2O$ (**2**). Yield 48%. $C_{24}H_{19}GdN_4NaO_{9.5}$ requires Gd 22.61%; found Gd 22.8%. M.Pt. > 250 °C (dec.).
$Na[Tb(pic)_4]\cdot 1.5H_2O$ (**3**). Yield 39%. $C_{24}H_{19}TbN_4NaO_{9.5}$ requires Tb 22.79%; found Tb 22.9%. M.Pt. > 250 °C (dec.).
$NH_4[Tb(pic)_4]\cdot 2H_2O$ (**4**). Yield 17%. $C_{24}H_{24}N_5O_{10}Tb$ requires Tb 22.75%; found Tb 22.7%. M.Pt. 305 °C (dec.).
$Na[Ho(pic)_4]\cdot 1.5H_2O$ (**5**). Yield 87%. $C_{24}H_{19}HoN_4NaO_{9.5}$ requires Ho 23.45%; found Ho 23.5%. M.Pt. > 250 °C (dec.).

X-ray crystallography studies

For all compounds X-ray quality crystals were sealed and mounted in thin walled capillaries, with hemispheres of data collected at room temperature on a Bruker SMART CCD diffractometer using the omega scan mode. Data sets were corrected for absorption using the program SADABS.[26] For all structures, the position of the heavy atoms were found using the Patterson method for heavy atoms and refined on F^2 using SHELXL97-2[27] with X-SEED as the graphic interface.[28] All non-hydrogen atoms were located and were refined with anisotropic thermal parameters. Hydrogen atoms were placed in calculated positions (riding model) and were not refined. For compound (**4**), hydrogen atoms of the NH_4^+ cation and water molecule were not located

from the difference map. Crystal data, and a summary of data collection are listed below, while selected bond distances and angles appear in the Tables.

Crystallographic data (excluding structure factors) for the structures reported in this paper have been deposited with the Cambridge Crystallographic Data Centre. CCDC-205568 for compound **1**, CCDC-205567 for compound **2**, CCDC-205569 for compound **3**, CCDC-205570 for compound **4** and CCDC-205571 for compound **5**. See http://www.rsc.org/suppdata/nj/b3/b302499g/ for crystallographic data in .cif or other electronic format.

Crystal refinement data

Crystal data for compound (1). $C_{48}H_{38}Eu_2N_8Na_2O_{19}$, $M = 1380.76$, $0.30 \times 0.30 \times 0.26$ mm, hexagonal, space group $P6_522$ (No. 179), $a = b = 12.6063(6)$, $c = 60.457(4)$ Å, $V = 8320.6(8)$ Å^3, $Z = 6$, $D_c = 1.653$ g cm^{-3}, $F_{000} = 4092$, MoKα radiation, $\lambda = 0.71073$ Å, $T = 296(2)$ K, $2\theta_{max} = 46.6°$, 38 011 reflections collected, 3987 unique ($R_{int} = 0.2096$). 0.2096). Final *GooF* = 1.308, *R*1 = 0.0787, *wR*2 = 0.1992, *R* indices based on 3975 reflections with $I > 2\text{sigma}(I)$ (refinement on F^2), 358 parameters, 168 restraints. Lp and absorption corrections applied, $\mu = 2.335$ mm^{-1}. Absolute structure parameter = 0.06(5).[29]

Crystal data for compound (2). $C_{48}H_{38}Gd_2N_8Na_2O_{19}$, $M = 1391.34$, $0.30 \times 0.30 \times 0.25$ mm, hexagonal, space group $P6_522$ (No. 179), $a = b = 12.5721(9)$, $c = 60.565(6)$ Å, $V = 8290.3(12)$ Å^3, $Z = 6$, $D_c = 1.672$ g cm^{-3}, $F_{000} = 4104$, MoK_α radiation, $\lambda = 0.71073$ Å, $T = 173(2)$ K, $2\theta_{max} = 46.6°$, 36 905 reflections collected, 3966 unique ($R_{int} = 0.1133$). 0.1133). Final *GooF* = 1.366, *R*1 = 0.0815, *wR*2 = 0.1822, *R* indices based on 3942 reflections with I > 2sigma(I) (refinement on F^2), 358 parameters, 168 restraints. Lp and absorption corrections applied, $\mu = 2.474$ mm^{-1}. Absolute structure parameter = 0.06(5).[29]

Crystal data for compound (3). $C_{48}H_{38}N_8Na_2O_{19}Tb_2$, $M = 1394.68$, $0.30 \times 0.25 \times 0.20$ mm, hexagonal, space group $P6_122$ (No. 178), $a = b = 12.5741(6)$, $c = 60.399(4)$ Å, $V = 8270.1(8)$ Å^3, $Z = 6$, $D_c = 1.680$ g cm^{-3}, $F_{000} = 4116$, MoKα radiation, $\lambda = 0.71073$ Å, $T = 296(2)$ K, $2\theta_{max} = 46.6°$, 38 255 reflections collected, 3953 unique ($R_{int} = 0.1793$). 0.1793). Final *GooF* = 1.077, *R*1 = 0.0604, *wR*2 = 0.1536, *R* indices based on 3650 reflections with I > 2sigma(I) (refinement on F^2), 358 parameters, 0 restraints. Lp and absorption corrections applied, $\mu = 2.640$ mm^{-1}. Absolute structure parameter = −0.01(3).[29]

Crystal data for compound (4). $C_{24}H_{24}N_5O_{10}Tb$, $M = 701.40$, $0.30 \times 0.30 \times 0.25$ mm, hexagonal, space group $P6_522$ (No. 179), $a = b = 12.7708(7)$, $c = 62.460(5)$ Å, $V = 8822.0(10)$ Å^3, $Z = 12$, $D_c = 1.584$ g cm^{-3}, $F_{000} = 4176$, $\lambda = 0.71073$ Å, $T = 296(2)$ K, $2\theta_{max} = 46.5°$, 40 197 reflections collected, 4206 unique ($R_{int} = 0.0864$). Final *GooF* = 1.344, *R*1 = 0.0982, *wR*2 = 0.2237, *R* indices based on 4166 reflections with I > 2sigma(I) (refinement on F^2), 363 parameters, 174 restraints. Lp and absorption corrections applied, $\mu = 2.464$ mm^{-1}. Absolute structure parameter = 0.12(6).[29]

Crystal data for compound (5). $C_{48}H_{38}Ho_2N_8Na_2O_{19}$, $M = 1406.70$, $0.30 \times 0.28 \times 0.22$ mm, hexagonal, space group $P6_522$ (No. 179), $a = b = 12.5245(18)$, $c = 60.470(12)$ Å, $V = 8215(2)$ Å^3, $Z = 6$, $D_c = 1.706$ g cm^{-3}, $F_{000} = 4140$, MoKα radiation, $\lambda = 0.71073$ Å, $T = 296(2)$ K, $2\theta_{max} = 46.6°$, 38 221 reflections collected, 3937 unique ($R_{int} = 0.0879$). 0.0879). Final *GooF* = 1.150, *R*1 = 0.0495, *wR*2 = 0.1231, *R* indices based on 3770 reflections with $I > 2\text{sigma}(I)$ (refinement on F^2), 352 parameters, 0 restraints. Lp and absorption corrections applied, $\mu = 2.964$ mm^{-1}. Absolute structure parameter = 0.03(3).[29]

Acknowledgements

We acknowledge the Australian Research Council for continued support. We also acknowledge an IPRS scholarship and Monash Graduate Scholarship (M.H.) and generous project funding by the DFG (D.S. subtopic within programme "Nanostructured host–guest systems").

References

1 J.-M. Lehn, *Supramolecular Chemistry*, VCH, Weinheim, 1995.
2 J. Kido, H. Nagai, Y. Okamoto and T. Skotheim, *Chem. Lett.*, 1991, 1267; H. Boerner, U. Kynast, W. Busselt and M. Haase, *EP* 0687 744 (1996), *USP* 5,756,334 (1998); D. Zhao, W. Li, Z. Hong, X. Liu, C. Liang and D. Zhao, *J. Luminescence*, 1999, **82**, 105; M. Baldo, M. E. Thomson and S. R. Forrest, *Nature*, 2000, **403**, 750; J. Kido and Y. Okamoto, *Chem. Rev.*, 2002, **102**, 2357.
3 G. F. de Sá, S. Alves, Jr., B. J. P. da Silva and E. F. da Silva, Jr., *Opt. Mater.*, 1998, **11**, 23.
4 J. C. Bünzli, in *Lanthanide Probes in Life, Medical and Environmental Science*, ed. G. R. Choppin, Elsevier, Amsterdam, 1989; Y. Shen and P. Sullivan, *J. Chem. Educ.*, 1997, **74**, 685.
5 N. Sabbatini, M. Guardigli and J.-M. Lehn, *Coord. Chem. Rev.*, 1993, **123**, 201.
6 O. A. Serra, E. J. Nassar, G. Zapparolli and I. L. V. Rosa, *J. Alloys Comp.*, 1994, **207/208**, 454; I. L. V. Rosa, O. A. Serra and E. J. Nassar, *J. Luminescence*, 1997, **72/73**, 263; M. Bredol, U. Kynast, M. Boldhaus and C. Lau, *Ber. Bunsenges, Phys. Chem.*, 1998, **102**, 1557; Y. Zhang, M. Wang and D. Wu, *J. Phys. Chem. Solids*, 1998, **59**, 1053; W. Strek, J. Sokolnicki, J. Legendziewicz, K. Maruszewski, R. Reisfeld and T. Pavich, *Opt. Mater.*, 1999, **13**, 41.
7 M. Bredol, U. Kynast and C. R. Ronda, *Adv. Mater.*, 1991, **3**, 361; M. Bredol, U. Kynast, C. R. Ronda and T. Welker, *EP* 0 522 627 (1994), *JP* 519 494 1 (1994); I. L. V. Rosa, O. A. Serra and E. J. Nassar, *J. Luminescence*, 1997, **72–74**, 532; D. Sendor and U. Kynast, *Adv. Mater.*, 2002, **14**, 1570; D. Sendor and U. Kynast,*Luminescence of Rare Earth metallo-organic complexes*, to appear in *Nanoporous Crystals*, eds. F. Laeri, F. Schüth, U. Simon and M. Wark, VCH-Wiley.
8 C. W. Newing, *USP* 3,367,910 (1968); A. V. Hayes and H. G. Drickamer, *J. Chem. Phys.*, 1982, **76**, 114; U. Kynast, *Paso GmbH, EP Appl.*, 02025915.6, (2002).
9 S. Sato and M. Wada, *Bull. Chem. Soc. Jap.*, 1970, **43**, 1955; W. R. Dawson, J. L. Kropp and M. Windsor, *J. Chem. Phys.*, 1966, **45**, 2410.
10 O. L. Malta, *J. Luminescence*, 1997, **71**, 229; F. R. G. de Silva and O. L. Malta, *J. Alloys Comp.*, 1997, **250**, 427.
11 G. F. de Sá, O. L. Malta, C. de Mello Donegá, A. M. Simas, R. L. Longo, P. A. Santa Cruz and E. F. da Silva, Jr., *Coord. Chem. Rev.*, 2000, **196**, 165.
12 H. G. Brittain, *Inorg. Chem.*, 1978, **17**, 2762; F. S. Richardson, *Chem. Rev.*, 1982, **82**, 541; H. G. Brittain, *J. Coord. Chem.*, 1990, **21**, 295.
13 S. Gruhlke and U. Kynast, *Electrochemical Society, Extended Abstracts of the 182nd meeting*, Honolulu, USA, 1993, 1348; D. Zhao, W. Li, Z. Hong, X. Liu, C. Liang and D. Zhao, *J. Luminescence*, 1999, **82**, 105; D. Zhao, Z. Hong, D. Zhao, X. Liu, W. Li, C. S. Lee and S. T. Lee, *Thin Solid Films*, 2000, **363**, 208.
14 A. Ouchi, Y. Suzuki, Y. Ohki and Y. Koizumi, *Coord. Chem. Rev.*, 1998, **92**, 29.
15 M. Jiang-Fang, H. Ning-Hai and N. Jia-Zuan, *Polyhedron*, 1996, **15**, 1797.
16 P. Starynowicz, *Acta Crystallogr.*, 1993, **C49**, 1895.
17 P. Starynowicz, *Acta Crystallogr.*, 1991, **C47**, 1897.
18 M. Johnson, J. C. Taylor and G. W. Cox, *J. Applied Crystallogr.*, 1980, **13**, 188.
19 R. D. Shannon, *Acta Crystallogr.*, 1976, **A32**, 751.
20 O. L. Malta, H. F. Brito, J. Menezes, F. R. Goncalves e Silva, C. de Mello Donega and S. Alves, Jr., *Chem. Phys. Lett.*, 1998, **282**, 233.

21 H.-Y. D. Ke and R. Birnbaum, *J. Luminescence*, 1995, **63**, 9.
22 B. W. van der Meer, G. Coker and S.-Y. S. Chen, *Resonance Energy Transfer*, VCH, 1994, ch. 2, 18.
23 M. F. Hazenkamp and G. Blasse, *Chem. Mater.*, 1990, **2**, 105.
24 For example see G. B. Deacon, T. Feng, P. C. Junk, B. W. Skelton and A. H. White, *Chem. Ber.*, 1997, **130**, 851.
25 T. Jüstel, D. U. Wiechert, C. Lau, D. Sendor and U. Kynast, *Adv. Funct. Mater.*, 2001, **11**, 105.
26 R. H. Blessing, *Acta Crystallogr.*, 1995, **A51**, 33.
27 G. M. Sheldrick, University of Gottingen, 1997.
28 L. J. Barbour, *X-SEED Crystallographic Interface*, 1999.
29 H. D. Flack, *Acta Crystallogr.*, 1983, **A39**, 876.